Theoretical study on the electric field effect on magnetism of Pd/Co/Pt thin films

Eszter Simon [*] Alberto Marmodoro,[†] Sergiy Mankovsky, and Hubert Ebert

Department Chemie/Phys. Chemie, Ludwig-Maximilians-Univerität München, Butenandtstrasse 5-13, D-81377 München, Germany

Recent x-ray magnetic circular dichroism experimental investigations on the magnetism of Pt overlayers deposited on ferromagnetically ordered Co films demonstrated the possibility of controlling the induced magnetic moment in Pt by applying an external electric field [Phys. Rev. Lett. **120**, 157203 (2018)]. Based on first-principles calculations, we investigate the electronic and magnetic properties of Pt layers in Pd(001)/Co/Pt thin film structures exposed to an external electric field. Due to the Co underlayer, the surface Pt layers have induced moments that are modified by an external electric field. The field-induced changes can be explained by the modified spin-dependent orbital hybridization that varies nonlinearly with the field strength. We calculate the x-ray absorption and the x-ray magnetic circular dichroism spectra for an applied external electric field and examine its impact on the spectra in the Pt layer around the L_2 and L_3 edges. We also determine the layer-dependent magnetocrystalline anisotropy, and we show that the anisotropy can be tuned easily in the different layers by the external electric field.

I. INTRODUCTION

The control of the magnetization of a system by an external electric field, which is known as the magnetoelectric effect, has been widely investigated during recent years experimentally as well as theoretically due to its potential application in spintronics [1–3]. The magnetoelectric effect was investigated in particular for bulk magnetic compounds with noncollinear magnetic structures [4–6], magnetic semiconductors [7,8], and multiferroics [9–12]. Within these studies, the modification of the magnetic properties by an external electric field has been associated with various electronic mechanisms, such as the shift of the Fermi level or a change in the charge-carrier density.

Recent studies have reported that an external electric field may affect the physical properties of layered systems in a very pronounced way [13,14]. For example, for thin films of Pd, it was shown that the electric field induces a phase transition from the para- to the ferromagnetic state. This finding could be explained by the Stoner instability caused by the applied electric field, which leads to a change in the occupation of the electronic states and shifting that way the Fermi level to a position with a high density of states (DOS). In the case of magnetic systems, an electric field changes their magnetic properties first of all due to its influence on the spin polarization of the valence electrons. Such a manipulation of the magnetic state by the electric field can lead to interesting and important effects concerning possible applications [15–17]. Performing first-principles calculations, it was demonstrated that a well-defined change in the magnetic moment can be observed in the case of a ferromagnetic free-standing thin Fe, Ni, or Co film, for which the magnetic moments show a linear dependence on the strength of the external electric field [18]. In this case, the electron populations in the different spin channels are varied and thus the balance of majority- and minority-spin electrons is distorted, leading in turn to a change of the spin magnetic moment in the system. Apart from the spin magnetic moment, many other magnetic properties may be controlled by an applied electric field, such as, for example, the orbital moment and its anisotropy as well as the magnetic anisotropy energy [18–20].

In the case of the Co/Pt bilayer system, it was demonstrated by means of anomalous Hall effect measurements that the Curie temperature of the Co layer can be controlled by an electric field [21]. For the Curie temperature of the bulk $3d$ transition metal alloys, a Slater-Pauling like behavior was found from first-principles calculations [22]. However, experimental results on thin films showed that the Curie temperature is increasing with an increasing number of valence electrons, and it does not follow the Slater-Pauling-like behavior [21]. This finding indicates that in the case of thin films—when compared to the bulk situation—other mechanisms can play an important role for the magnetic properties in the presence of an electric field.

Paramagnetic metals, such as Pt and Pd, that are close to the Stoner instability, have substantial induced moments due to the proximity effect when deposited on magnetic substrate layers. In the case of Pd deposited on the Pt/Co bilayer system, it was demonstrated experimentally and theoretically that the induced magnetic moment of the Pd layer can be controlled by an applied electric field [14]. The interrelation between the influence of an electric field on the magnetic state and the electronic structure of Pt deposited on a magnetic substrate was investigated in a recent work by exploiting the component-specific x-ray absorption spectroscopy (XAS) together with the x-ray magnetic circular dichroism (XMCD) [13].

———————
*Eszter.simon@cup.uni-muenchen.de

†Present address: Institute of Physics, Czech Academy of Sciences, Cukrovarnicka 10, CZ-162 53 Prague, Czech Republic.

XMCD is one of the most powerful probes for investigating the magnetization of layered systems in an element-resolved way [23]. The XMCD spectra give for a magnetized sample the difference in absorption for left- and right-circularly-polarized x rays. XMCD spectra are often analyzed on the basis of the XMCD sum rules, which link the integrals of the XAS and XMCD spectra to the spin and orbital magnetic moments of the absorbing atom [24–28].

Motivated by a recent experimental XMCD study by Yamada *et al.* [13], we investigated the electronic and magnetic properties of Pt layers in the surface film system Pd(001)/Co/Pt in the presence of an external electric field by means of first-principles calculations. In this way, we investigated how the electric field influences the electronic states, the magnetic moments, the XMCD spectra of the Pt layers, and the magnetic anisotropy in the case of the considered systems.

The paper is organized as follows. In Sec. II, the computational methods used are briefly sketched, while in Sec. III the results are presented and discussed. Finally, in Sec. IV we summarize our results.

II. COMPUTATIONAL DETAILS

All calculations were performed within the framework of density functional theory, relying on the local-spin-density approximation (LSDA). For the exchange correlation potential, the parametrization of Vosko, Wilk, and Nusair was used [29]. The electronic structure is described on the basis of the Dirac equation, accounting for all relativistic effects coherently this way. Electronic states were represented by means of the corresponding Green function calculated using the spin-polarized Korringa-Kohn-Rostoker (KKR) Green function formalism as implemented in the spin-polarized relativistic KKR (SPR-KKR) code [30–32]. The potentials were treated on the level of the atomic sphere approximation (ASA), and for the self-consistent calculations an angular momentum cutoff of $l_{max} = 3$ was used. All necessary energy integrations have been done by sampling 32 points on a semicircle contour in the upper complex energy semiplane. Furthermore, the **k**-space integration over the two-dimensional Brillouin zone (BZ) was done using a 109×109 two-dimensional (2D) k-mesh.

We investigated the Pd(001)/Co$_n$/Pt$_m$ thin film surface system, where n and m denote the number of Co and Pt layers, respectively. The first considered model system consisted of three Pd layers, $n = 2$ or 5 Co layers, $m = 2$ Pt layers, and three layers of empty spheres embedded between a semi-infinite Pd substrate and a semi-infinite vacuum region. For the second model system, the number of Pt layers was varied with the system consisting of two Pd, $n = 5$ Co layers, $m = 1, 4$ Pt layers, and three layers of empty spheres embedded between the semi-infinite Pd and vacuum regions. For Pd, Co, Pt, and empty layers, ideal epitaxial growth was assumed on a fcc(001) textured substrate with the experimentally in-plane lattice constant of Pd, $a_0 = 3.89$ Å. Structural relaxations were neglected in all cases.

From the obtained self-consistent potentials, the x-ray absorption coefficients $\mu_\lambda(\omega)$ for the photon energy $\hbar\omega$ and polarization λ were calculated using the SPR-KKR Green function method on the basis of Fermi's Golden Rule [30,33].

The corresponding XMCD signal,

$$\Delta\mu(\omega) = \tfrac{1}{2}(\mu_+(\omega) - \mu_-(\omega)), \qquad (1)$$

is defined as the difference in the absorption for left and right circularly polarized radiation. The broadening of the experimental spectra was simulated by a Lorentzian broadening function with a width parameter of 1 eV.

The magnetic anisotropy energy (MAE) was obtained by means of magnetic torque calculations [34,35] giving in general an access to the magnetic torque $T(\theta, \phi)$ as a function of the polar and tangential angles θ and ϕ. Following Staunton *et al.* [34], for uniaxial magnetic anisotropy the angle dependency of the energy can be evaluated using the torque at $\theta = \pi/4$ and $\phi = 0$ (assuming weak in-plane anisotropy), i.e., $E_{100} - E_{001} = T(\theta = \pi/4, \phi = 0)$. Some details of the magnetic torque calculations are represented in Appendix.

The effect of a homogeneous external electric field was modeled by a periodic array of point charges in the vacuum region that behave essentially like a charged capacitor plate. In the present calculations, the array of point charges or capacitor plate, respectively, was placed in the last vacuum layer. This setup leads to a homogeneous electric field of strength

$$E = \frac{Q}{a_0^2 \epsilon_0}, \qquad (2)$$

where Q is the charge of the capacitor in units of the electron's charge, ϵ_0 is the permittivity of vacuum, and a_0^2 is the area of the unit cell for the Pd(001) plane. Here, the applied electric field is perpendicular to the surface, and for the positively charged condensed plate it points from the vacuum toward the surface, increasing this way the spill-out of the electrons from the Pt layers to the vacuum with increasing electric field strength.

III. RESULTS

A. Variation of the thickness of the Co layer

To investigate the impact of an external electric field on the electronic structure of the Pd(001)/Co$_n$/Pt$_m$ system, we focus first on Pd(001)/Co$_2$/Pt$_2$ with a ferromagnetically ordered Co film, corresponding essentially to a system composed of 0.5 nm Co and 0.4 nm Pt films, as studied recently in Ref. [13]. These experiments have been accompanied by theoretical work, however, considering in contrast to the present study a (111)-oriented surface. From the self-consistent calculations, we obtained the spin magnetic moments of the layers as a function of the electric field. The spin magnetic moments of the Co layers without an external electric field ($E = 0$) are $m_{Co_1} = 1.92 \, \mu_B$ and $m_{Co_2} = 1.89 \, \mu_B$, showing a trend well established for the thickness-dependent properties of ultrathin magnetic films.

To see an impact of the thickness of the ferromagnetic film on the spin and orbital polarization of the Pt film, the calculations have been performed also for Pd(001)/Co$_5$/Pt$_2$. In this case, the magnetic moments for four Co layers (for $E = 0$) are very close to each other, $m_{Co_2} \sim m_{Co_3} \sim m_{Co_4} \sim m_{Co_5} \sim 1.8 \, \mu_B$, while for the Co layer at the Pd/Co interface the magnetic moment is the largest one, $m_{Co_1} \sim 1.9 \, \mu_B$.

When the thickness of the ferromagnetic layer increases, the spin magnetic moment in the middle of the
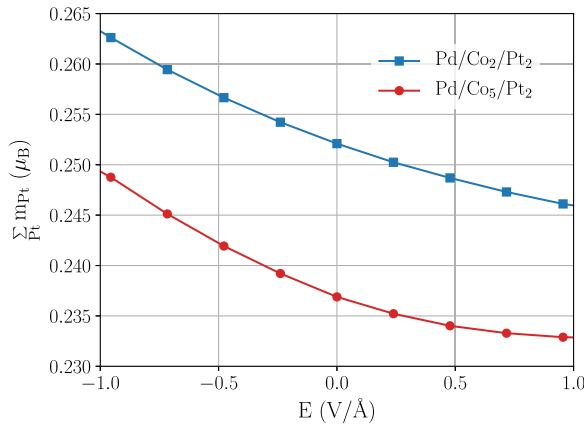
FIG. 1. Calculated sum of the spin magnetic moment of the Pt layers, $\sum_{Pt} m_{Pt}$, as a function of the external electric field E for Pd(001)/Co$_2$/Pt$_2$ (squares) and Pd(001)/Co$_5$/Pt$_2$ (circles).

FIG. 2. Calculated spin-polarized density of states, $n^{\uparrow(\downarrow)}(\varepsilon, \pm E)$, projected to s, p, and d states for the topmost Pt layer in Pd(001)/Co$_2$/Pt$_2$ for the selected electric fields $E = \pm 7$ V/nm indicated by $\pm E$.

film approaches the value corresponding to the three-dimensional bulk material, while the magnetic moment at the interface/surface remains different, as a consequence of the different arrangement for these atoms. Note that in the case of the Pd(001)/Co$_5$/Pt$_2$ system, the magnetic moment of the central layer is larger when compared to that of bulk fcc Co, being a consequence of the larger lattice parameter corresponding to fcc Pd in the systems under discussion. At the Co/Pt interface, the magnetic moment is quite close to that obtained for the central layer of the Co film, while at the Pd/Co interface the Co magnetic moment is the largest one. For both systems, the change of the magnetic moment of the Co layers induced by the electric field is negligible.

In the Pt layers, induced spin moments are formed due to the proximity effect caused by the Co layer with the value of the induced moment being largest for the Pt layer at the Pt/Co interface. In the presence of the external electric field, the magnetic moments in the Pt film are modified. Despite the small difference in the Pt spin moments, this modification is similar for two systems with different Co thickness, as can be seen in Fig. 1 showing the sum of the spin magnetic moments of the Pt layers, $\sum_{Pt} m_{Pt}$, as a function of the electric field for both considered systems.

For both systems, the magnetic moment decreases with increasing positive electric field in spite of the different number of Co layers. Moreover, in contrast to calculations for free-standing ferromagnetic thin films [18], the Pt spin magnetic moment in the present case does not vary linearly with the field strength.

To understand the variation of the Pt spin magnetic moment in the presence of the electric field, we calculated the density of states (DOS) for the topmost Pt layer in the case of two opposite signs of electric field, and we compared their effect with the zero electric field ($E = 0$). Figure 2 shows for various electric field strengths the spin-resolved DOS projected onto s, p, and d states for the topmost Pt layer in Pd(001)/Co$_2$/Pt$_2$. The applied electric field strengths have the value ± 7 V/nm, denoted as $+E$ and $-E$ in the following. One can see that the external electric field slightly modifies the electronic states of the Pt layer. A positive electric field shifts the s, p, as well as d states of Pt down, while a negative field shifts the states up in
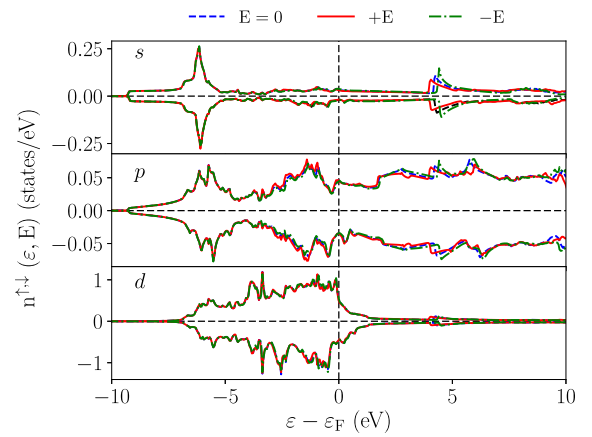
energy. Moreover, one can see that these shifts increase with the energy of the electronic states as they are more affected by the electric field due to their weaker localization. Due to the difference of the DOS for the two spin channels, these shifts lead to a change of the magnetic moments, which depend on the sign of the electric field.

To see in more detail the changes of the band structure induced by an external electric field, we represent the Bloch spectral function (BSF), $A(\mathcal{E}, \vec{k})$, in the vicinity of the Fermi level. Figure 3 shows the difference of the Bloch spectral functions in the presence of the electric field, positive ($E = -7$ V/nm) or negative ($E = 7$ V/nm), and one calculated for zero electric field, $A(\mathcal{E}, \vec{k}, \pm E) - A(\mathcal{E}, \vec{k}, 0)$: the top and middle panels represent the states projected onto the Pt$_2$ and Pt$_1$ layers, and the bottom panel represents the projection of the states onto the topmost Co layer in the Pd(001)/Co$_2$/Pt$_2$ system. According to the chosen color scale, the red and blue colors indicate the highest and lowest values of the BSF difference, meaning modified and not modified states, respectively. As one can see, the electric field results in a shift of the electronic states localized in the surface Pt layers where the field screening is only moderate. Depending on the sign of the electric field, the shift occurs either up or down in the case of $-E$ (left panels) and $+E$ (right panels), respectively. The shift of the electronic states in the Pt layers is accompanied by an apparent smearing due to a change of their hybridization with Co electronic states in the interface region, as Fig. 3 shows. The most pronounced changes of the electronic structure in the Co layers are a consequence of such a "rehybridization." The bulk states are not affected by the electric field at all, and the shift of the states localized far away from the surface decreases due to the decay of the screened electric field.

To discuss the origin of the changes of the induced spin magnetic moments in the Pt layers in the presence of an applied electric field, the BSF is plotted in Fig. 4 showing the corresponding changes of the majority- (top panel) and minority-spin (bottom panel) states in the interface Pt layer (Pt$_1$). On the one hand, a general similarity of these changes for two different spin channels can be seen. This implies
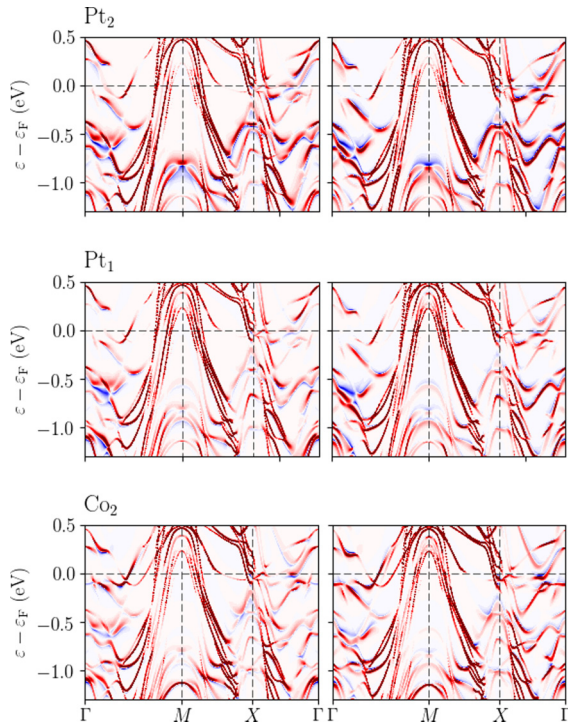
FIG. 3. Calculated Bloch spectral function, $A(\mathcal{E}, \vec{k}, E) - A(\mathcal{E}, \vec{k}, 0)$, demonstrating the field-induced changes of the electronic structure for the Pd(001)/Co$_2$/Pt$_2$ system in Pt$_2$ (top panel), Pt$_1$ (middle panel), and Co$_2$ (bottom panel) layers. The difference for negative ($E = -7$ V/nm) and positive ($E = 7$ V/nm) electric field are shown in the left and right panels, respectively. Red and blue correspond to modified (highest values) and not modified (lowest value).
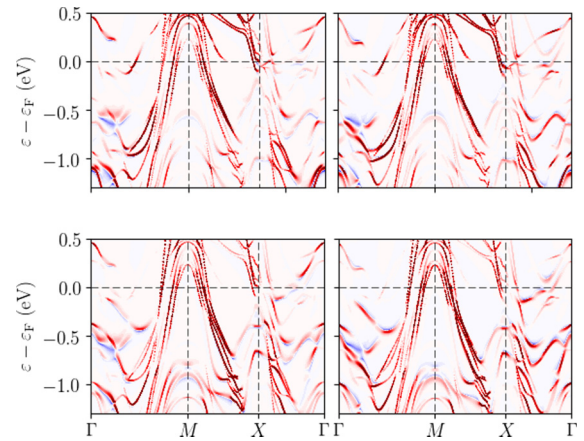

FIG. 4. Calculated spin-resolved Bloch spectral function, $A(\mathcal{E}, \vec{k}, E) - A(\mathcal{E}, \vec{k}, 0)$, representing the field-induced changes of the majority-spin (top panel) and minority-spin (bottom panel) states in the Pt$_1$ layer (at the Pt/Co interface) in the case of the Pd(001)/Co$_2$/Pt$_2$ system, The difference for negative ($E = -7$ V/nm) and positive ($E = 7$ V/nm) electric field are plotted in the left and right panels, respectively. Red and blue correspond to modified (highest values) and not modified (lowest value).

in turn a rather weak difference between the majority- and minority-spin states affected by the electric field, which may be associated with weakly spin-polarized Pt states. On the other hand, one can see the difference in the BSF modifications in Fig. 4, which is a result of spin-dependent hybridization of the Pt states with the majority- and minority-spin states of Co. This different "rehybridization" leads in turn to the changes of induced Pt spin magnetic moments in the presence of an electric field.

It should be noted that in contrast to the work on a free-standing film in Ref. [13], the Fermi level is fixed as we deal with a half-infinite substrate for which the electric field effectively acts only on the surface. Accordingly, the value of the Fermi energy is that of the Pd substrate for all applied electric fields.

Another effect of the electric field seen in Fig. 2 is the change of the amplitude of the DOS due to the change of hybridization of the electronic states of Pt and Co layers, or as was pointed out in Ref. [13], the hybridization of the sp-states and the d-states of Pt. As the hybridization is spin-dependent, this also results in a change of the magnetic moments induced by the electric field.

As discussed in the literature [13], the above-mentioned field-induced changes of the electronic structure and magnetic properties can be probed in a detailed way using XAS/XMCD spectroscopy. Focusing here on the magnetic properties of the Pt layers, the absorption spectra at the Pt L_2 and L_3

edges have been calculated both for Pd(001)/Co$_2$/Pt$_2$ and Pd(001)/Co$_5$/Pt$_2$. The XAS and XMCD spectra without the influence of an external electric field are given in Fig. 5, showing only tiny differences between the two systems.

The modifications of the XAS spectra for these systems by the electric field $\pm E$ are represented in Fig. 6, showing the field-induced changes, $\mu(\pm E) - \mu(0)$, of the total XAS and of XMCD signals, $\Delta\mu(\pm E) - \Delta\mu(0)$, for the Pt layers in Pd(001)/Co$_2$/Pt$_2$ and Pd(001)/Co$_2$/Pt$_4$. Although only tiny differences are found for both systems, one can see that the changes are most pronounced at the L_3 edge in both cases. This finding is in line with the previously reported experimental results [13], and it can be explained as follows. As an electric field will in particular shift electronic states below or above the Fermi level, pronounced field-induced changes
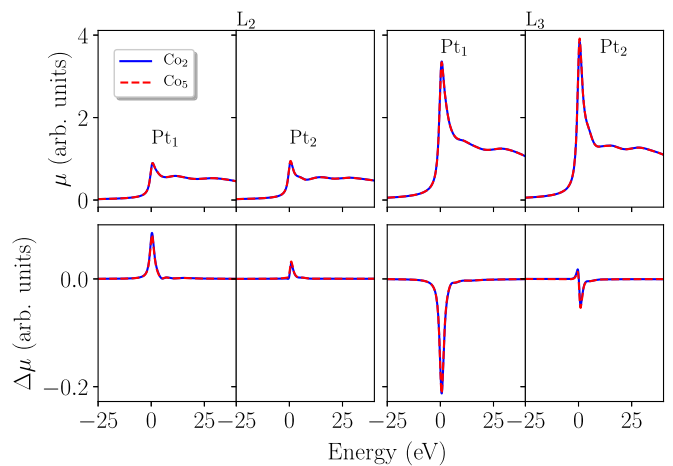

FIG. 5. Calculated layer-resolved XAS (top panel), μ and XMCD (bottom panel), $\Delta\mu$ spectra at the L_2 and L_3 edges for the Pt layers in Pd(001)/Co$_2$/Pt$_2$ (solid line) and Pd(001)/Co$_5$/Pt$_2$ (dashed line).
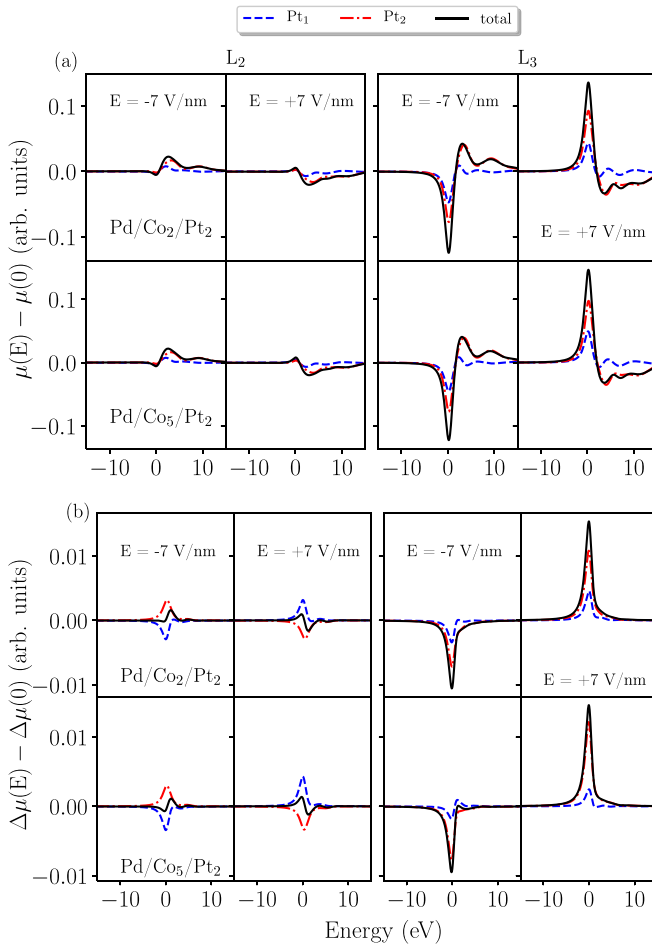
FIG. 6. Difference of the calculated layer-resolved XAS (a) and XMCD (b) spectra of Pt layers between in the absence and presence of an electric field, $\mu(\pm E) - \mu(0)$, $\Delta\mu(\pm E) - \Delta\mu(0)$, around L_2 and L_3 edges in the case of $Pd(001)/Co_2/Pt_2$ and $Pd(001)/Co_5/Pt_2$ systems.

have to be expected first of all at the absorption edges of the spectra. As the Pt d-states in that energy region have primarily $d_{5/2}$-character, and as the L_3 and L_2 spectra are dominated by their $d_{5/2}$- and $d_{3/2}$-contributions, respectively, it follows that an electric field has a much stronger impact for the L_3 than for the L_2 spectrum.

The modifications of XAS and XMCD spectra depend directly on the direction of the electric field as this determines the direction of the field-induced shift of the electronic states with respect to the Fermi energy. Due to the screening of the electric field with increasing distance from the surface, the field-induced changes of the XAS and XMCD signals are most pronounced for the surface Pt layer and decrease toward the interface. This behavior can be seen clearly in Fig. 6 showing the layer-resolved results for $Pd(001)/Co_2/Pt_2$. The same trend is found also for $Pd(001)/Co_5/Pt_2$. Note that in Ref. [13], the same findings for the electric field induced change of the spin magnetic moments of Pt, XMCD, and XAS spectra were obtained for the (111) orientation, indicating that in the case of the present considered system, the electric field effect is independent of the layer orientation.

TABLE I. Sum of the spin magnetic moment of the Pt layers, $\sum_{Pt} m_{Pt}$, obtained by the sum rules and from the self-consistent calculation in the case of the $Pd(001)/Co_2/Pt_2$ system for zero electric field and two different signs of external electric fields, E.

E (V/nm)	$\sum_{Pt} m_{Pt}(\mu_B)$	
	From sum rules	From DFT calc.
+7	0.135	0.246
0	0.139	0.252
−7	0.143	0.259

Using the XMCD spin sum rule, the spin magnetic moments can also be obtained from the calculated XMCD spectra. In the case of the $Pd(001)/Co_2/Pt_2$ system, we compared the sum of the calculated self-consistent spin magnetic moment of the Pt layers, $\sum_{Pt} m_{Pt}$, with the obtained values from the sum rules. Table I summarizes the corresponding results for two different signs of the external electric field and for zero field. Obviously, the spin magnetic moment of the Pt layer determined from the sum rules shows the same trend as a function of the electric field as the results obtained from self-consistent calculation. The findings represented in Table I are fully in line with the general experience that the obsolete values for the moments obtained by the XMCD sum rules may depend on the normalization of the spectra. Comparing different systems, however, the trend is always correct. This applies in particular in cases with small moments. Finally, it should be mentioned that we restricted our examination here to the spin moment as the changes of the XMCD spectra with an electric field, because these variations are too small to apply the XMCD orbital sum rule in a reliable way.

B. Variation of the thickness of the Pt layer

To investigate how the electric field effect changes with an increasing thickness of the Pt film, calculations have been performed for the $Pd(001)/Co_5/Pt_m$ system, where the thickness of the capping Pt layer was varied between $m = 1$ and 4. The top panel of Fig. 7 shows the calculated spin moments of the individual layers in $Pd(001)/Co_5/Pt_1$ (a) and $Pd(001)/Co_5/Pt_4$ (b) for various electric fields. In the case of $Pd(001)/Co_5/Pt_1$, the Pt spin moment is $m_{Pt_1} = 0.22 \, \mu_B$. For $Pd(001)/Co_5/Pt_4$, the induced moment of the Pt layers significantly decreases away from the Co interface while the Pt layer at the Co interface possesses the largest induced moment with $m_{Pt_1} = 0.18 \, \mu_B$ coupled ferromagnetically to that of Co. The spin magnetic moment of the next Pt layer is $m_{Pt_2} = 0.06 \, \mu_B$ and is also ferromagnetically aligned to the Co moments. The remaining very small magnetic moments for the third and fourth Pt layers are antiferromagnetically oriented with respect to the Co layers.

The Pt spin magnetic moment in $Pd(001)/Co_5/Pt_1$ increases in the case of a positive electric field $(+E)$ while it decreases for $-E$ with the value $0.23 \, \mu_B$ and $0.21 \, \mu_B$, respectively. This dependency on the electric field is opposite to that of $Pd(001)/Co_n/Pt_2$ shown in Fig. 1, and it can be attributed to the screening of the electric field that gets more important for an increasing thickness of the Pt film.
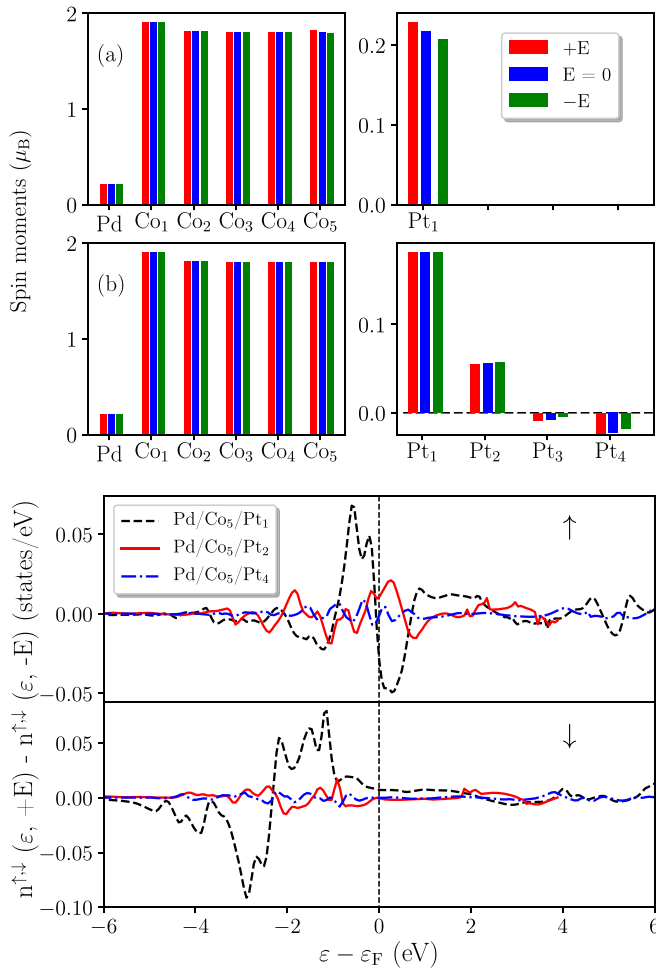
FIG. 7. Top panel: Calculated layer-resolved magnetic spin moments of the individual atomic layers in Pd(001)/Co$_5$/Pt$_1$ (a) and Pd(001)/Co$_5$/Pt$_4$ (b) without electric field and in the presence of a positive and negative electric field. Bottom panel: Calculated difference for the minority and majority density of states of the interface Co layer between positive and negative electric field for different thicknesses of the capping Pt layer.

In particular, one can see rather strong field-induced changes of the spin magnetic moments of the interface and next-to-interface Co layers in Pd(001)/Co$_5$/Pt$_1$. In this case, the spin moment of the Pt layer follows the changes of the spin moment of Co at the Co/Pt interface. Obviously, the impact of the electric field on the Co spin moment significantly decreases with the increasing thickness of the Pt film. The bottom panel in Fig. 7 shows the difference in the density of states for majority and minority spins of the topmost Co layer (Co$_5$) obtained for different electric fields. These electric-field-induced changes in the DOS are decreasing for the Co layers when the thickness of the Pt film increases. This screening effect is also seen in the bottom panel of Fig. 8, which represents the field-induced DOS and the spin density changes in the different Pt layers of Pd(001)/Co$_5$/Pt$_4$.

One can see that the most pronounced DOS changes due to an applied electric field occur in the surface Pt layer, while the DOS modification in the deeper Pt layer and at the Pt/Co interface is rather weak (see the top panel of
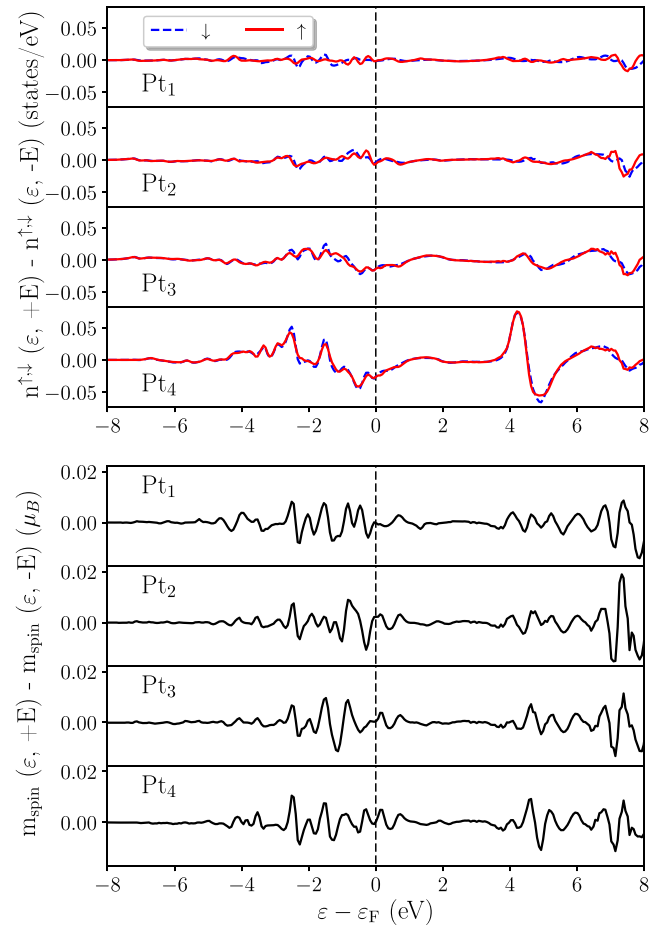

FIG. 8. Top panel: Electric-field-induced change of the density of states in the different Pt layers in Pd(001)/Co$_5$/Pt$_4$. Bottom panel: Electric-field-induced change of the difference $m_{\mathrm{spin}} = n^{\uparrow}(\varepsilon) - n^{\downarrow}(\varepsilon)$ of majority and minority DOS.

Fig. 8). Despite this trend, the bottom panel of Fig. 8 shows that the field-induced changes of the spin polarization [i.e., $m_{\mathrm{spin}}(\varepsilon) = n^{\uparrow}(\varepsilon) - n^{\downarrow}(\varepsilon)$] have the same order of magnitude for all Pt layers. This can be attributed to the strongest field effect for the surface Pt layer on the one hand and the strongest proximity-induced spin moment at the interface on the other hand.

Thus, one can conclude that depending on the thickness of the Pt layer, the field-dependent changes of the induced spin moment can be dominated by different mechanisms associated with field-induced changes of the electronic structure and magnetic moments either in the ferromagnetic subsurface or in the nonmagnetic surface parts of the system.

Next, we discuss the influence of the electric field on the XAS and XMCD spectra at the L_2- and L_3-edges of Pt in Pd(001)/Co$_5$/Pt$_n$ with $n = 1$ and 4 and its dependence on the thickness n of the Pt film. First, we consider in Fig. 9 (top panel) the layer-resolved XAS spectra calculated without including an external electric field. One can see a weak dependence of the XAS spectra on the position of the Pt layer in the Pd(001)/Co$_5$/Pt$_4$ system. However, the XMCD spectra shown in Fig. 9 (bottom panel) exhibit a rather pronounced decrease when going from the interface (Pt$_1$) to the surface
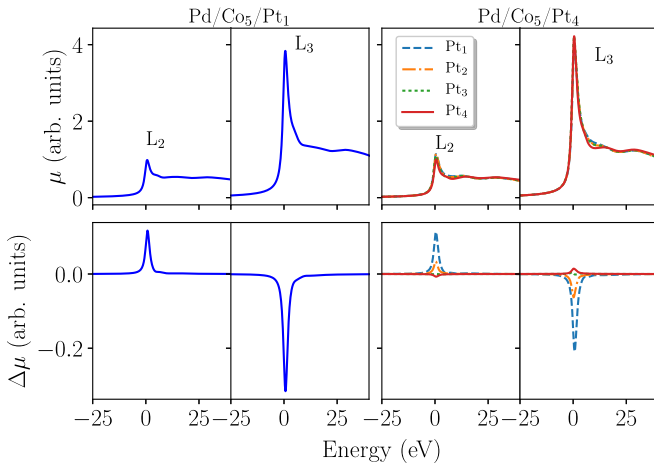
FIG. 9. Calculated layer-resolved XAS (top panel) μ and XMCD (bottom panel) $\Delta\mu$ spectra at the L_2- and L_3-edges for the Pt layers in Pd(001)/Co$_5$/Pt$_1$ (left) and Pd(001)/Co$_5$/Pt$_4$ (right).

(Pt$_4$) layer. Note that the XMCD signal of the surface Pt layer even changes sign in line with the sign change for the induced spin moment in this layer (see the discussion above). The strongest XMCD signal occurs for the interface Pt layer reflecting the largest induced spin moment due to its proximity to the ferromagnetically ordered Co layers.

The changes of the XAS and XMCD spectra of Pt in Pd(001)/Co$_5$/Pt$_1$ and Pd(001)/Co$_5$/Pt$_4$ that are caused by the applied electric field are presented in Figs. 10(a) and 10(b), respectively. Similar to the systems with 2 monolayer (ML) of Pt, one finds that the change of the spectra reverses its sign if the orientation of the electric field is reversed. In addition, one can see the asymmetry of these modifications with respect to a change in the orientation of the electric field. The most pronounced changes occur for the Pt L_3 edge signal, similar to the results obtained for Pd(001)/Co$_2$/Pt$_2$. The intensities of the layer-resolved changes of the XAS spectra for Pt in Pd(001)/Co$_5$/Pt$_4$ gradually decrease when going from the Pt surface to the interface layer. As discussed above, this can be attributed to the screening of the electric field in the surface region. However, the XMCD spectra change nonmonotonously toward the interface layer as a consequence of a competition of the decreasing electric field strength and the increasing impact of the neighboring Co layers controlling the Pt spin magnetic moment via the proximity effect.

In addition to the impact of an electric field on the XMCD spectra, its influence on the layer-resolved MAE was investigated. Figure 11 shows the layer-resolved MAE of Pd(001)/Co$_5$/Pt$_1$ and Pd(001)/Co$_5$/Pt$_4$, respectively, for no electric field present as well as for an applied electric field with positive and negative sign, respectively. The definition for the MAE used implies an out-of-plane and in-plane anisotropy for a positive or negative sign, respectively, of the MAE.

First, let us discuss the variation of the MAE for these systems without an external electric field, focusing on the layer-resolved contributions to the total MAE (see more details in Appendix). One can see a strong decrease of the contribution from Pt and an increase of the contribution from
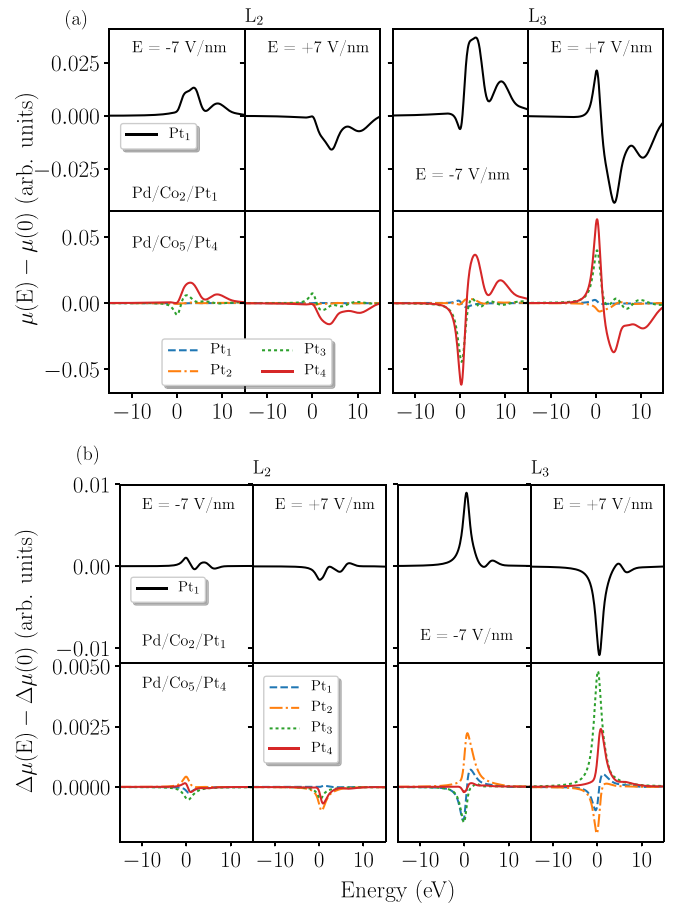

FIG. 10. Electric-field-induced change in the XAS (a) and XMCD (b) spectra at the L_2 and L_3 edges for Pt in Pd(001)/Co$_5$/Pt$_1$ and Pd(001)/Co$_5$/Pt$_4$.

Co interface layers in the case of Pd(001)/Co$_5$/Pt$_4$ compared to Pd(001)/Co$_5$/Pt$_1$. An increase of the MAE in alloys and compounds containing heavy-element atoms occurs due to hybridization of $3d$-states of magnetic and $5d$-states of nonmagnetic atoms, discussed, for example, in Ref. [36]. In the case of layered systems, such a hybridization effect at the interface between magnetic and heavy-element films can lead to a strong enhancement of the uniaxial MAE of the system (see, e.g. Refs. [37,38]). The dependence of the MAE on the thickness of the magnetic as well as nonmagnetic films was discussed by different groups [37,39–44], considering it in particular with the thickness-dependent quantum-well states in the films that may occur. However, to the best of our knowledge only a few reports exist in the literature discussing the layer-resolved contributions to the MAE [40,42]. It is well known that the MAE is strongly determined by the electronic states near the Fermi energy, ε_F. A variation with a film thickness of the layer contributions to the MAE is caused by a shift of these states with respect to ε_F and by a change of their localization in different atomic layers. These effects are responsible for the change of the contributions from the interface layers, caused by the change of the Pt film thickness. As one can see in Fig. 11, the Pt interface contribution decreases and the Co contribution increases when the Pt thickness increases from $m = 1$ to 4, which leads accidentally to a large
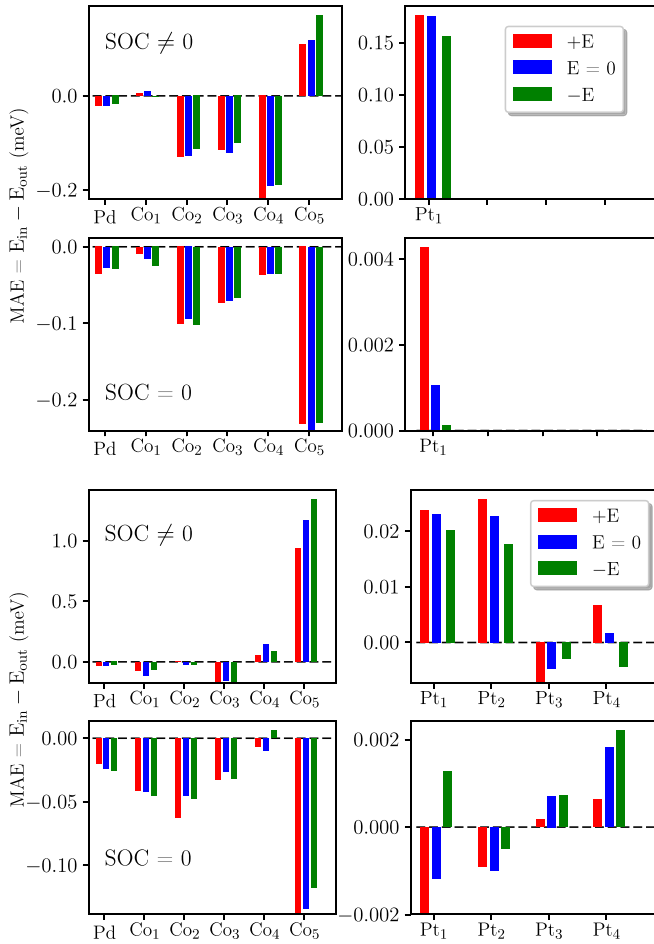
FIG. 11. Calculated layer-resolved magnetic anisotropy energy (MAE) of $Pd(001)/Co_5/Pt_1$ (top panels) and $Pd(001)/Co_5/Pt_4$ (bottom panels) for no electric field present as well as for an applied electric field with positive and negative sign, respectively. The results have been obtained from fully relativistic calculations (SOC $\neq 0$) and calculations with the strength of the spin-orbit coupling in the Pt layers set to zero (SOC $= 0$).

FIG. 12. Top panel: Contribution to the magnetic anisotropy energy from the Co_5 and Pt layers (without SOC scaling and with SOC $= 0$ in the Pt layers), represented as a function of occupation of energy bands in the case of the $Pd(001)/Co_5/Pt_1$ system. Bottom panel: Field-induced changes of the contribution to the magnetic anisotropy energy from the Co_5 layer, MAE($\pm E$) $-$ MAE(0).

MAE corresponding to an in-plane anisotropy with dominating contributions from the Co layers in the middle of the Co film, while the positive contribution from the interface Co/Pt layer is rather small. $Pd(001)/Co_5/Pt_4$, on the other hand, has out-of-plane anisotropy with its MAE dominated by the contribution from the Co layer at the Co/Pt interface. It should be noted that a strong dependence of the MAE on the thickness of the overlayer was discussed already for several systems [46,47]. Figures 12 and 13 illustrate the contributions to the MAE from the interface Co and Pt layers, represented as a function of the occupation of the valence band realized by artificially varying the Fermi energy.

These relations have a nonmonotonous behavior with extreme values always occurring when the Fermi energy is passing through a SOC-induced avoided crossing of the

difference in the latter case. Note that a similar trend has been reported for the Pt-decorated Co clusters [45] deposited on Pt(111) with a leading contribution of the Co rim at the Co/Pt interface, despite a weak SOC of Co atoms when compared to that of Pt.

In an earlier study [19], it was already found that an electric field may strongly affect the magnetocrystalline anisotropy of free-standing transition metal monolayers as a result of the distortion of the electronic structure by the applied electric field. The authors point out that in these systems, the electric field breaks the z-reflection symmetry, lifting in that way a degeneration in the cross-points of the energy bands via the field-induced hybridization between the d and p orbitals that contribute to these states.

As Fig. 11 illustrates, an electric field also strongly modifies the MAE for the systems considered here despite the lack of z-reflection symmetry for the field-free case. As a reference, the figure also shows the total and layer-resolved MAE for $Pd(001)/Co_5/Pt_1$ and $Pd(001)/Co_5/Pt_4$ for zero-field conditions. As one can see, $Pd(001)/Co_5/Pt_1$ has a total
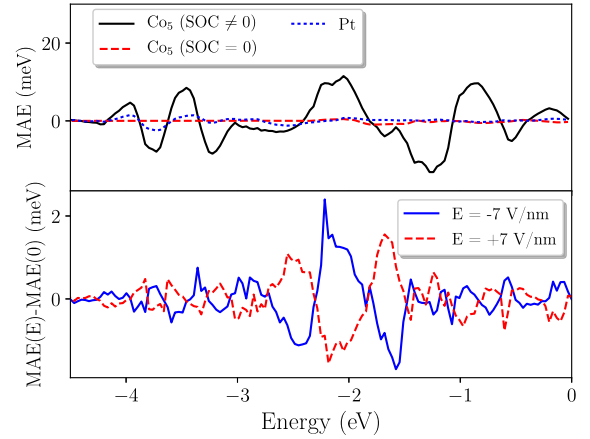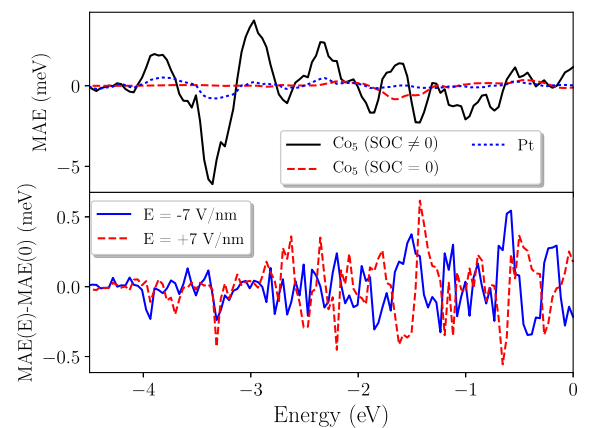

FIG. 13. Top panel: Contribution to the magnetic anisotropy energy from the Co_5 and Pt layers (without SOC scaling and with SOC $= 0$ in the Pt layers), represented as a function of occupation of energy bands in the case of the $Pd(001)/Co_5/Pt_4$ system. Bottom panel: Field-induced changes of the contribution to the magnetic anisotropy energy from the Co_5 layer, MAE($\pm E$) $-$ MAE(0).

energy bands. One can see that for both systems, the amplitude of the contribution to the MAE associated with the Co interface layer is much larger than that for the Pt interface layer. However, accidentally, these values can be close to each other at a certain occupation, as is the case for $Pd(001)/Co_5/Pt_1$ at the proper Fermi energy. It should be noted that the MAE of materials composed of magnetic- and heavy-element components is determined essentially by the spin-dependent hybridization of their electron orbitals as well as by the SOC of the heavy element (see, for example, Refs. [36,48,49]). As the $Pd(001)/Co_5$ substrate is common to both systems considered, the difference in the MAE has to be attributed to the details of the electronic structure of these systems associated with a different thickness of the Pt surface film. As a result, artificially switching off the SOC on the Pt atoms leads for the Pt film to a strong weakening of the dependence of its electronic structure on the magnetization direction and in turn of the MAE. This is seen in Figs. 12 and 13, indicating that the contribution of the Co interface layer to MAE drops down by about one order of magnitude when the SOC is switched off for Pt. For this situation, the layer-resolved MAE for both systems is rather similar (see Fig. 11). The difference between the results for the two systems can be attributed to some extent to a different hybridization of the Co- and Pt-related electronic states, which is obviously dependent on the thickness of the Pt film. Based on these results, one can expect that the field-induced changes to the MAE should be associated first of all to the influence of the electric field on the Pt-related electronic states.

Analyzing the field-induced changes of the total and layer-resolved MAE of $Pd(001)/Co_5/Pt_1$ and $Pd(001)/Co_5/Pt_4$, the most pronounced changes are found at the interface, although the changes for the other layers are not negligible. Despite the pronounced screening effect in the case of $Pd(001)/Co_5/Pt_4$ with 4 ML of Pt, the field-induced change of the Co interface contribution to the MAE is significant, indicating a key role of the electronic structure changes occurring in the Pt film due to the electric field. The field-induced changes of the MAE in the systems with 1 and 4 ML of Pt are associated primarily with the Co/Pt interface contribution. Corresponding results for the interface layers are plotted in Figs. 12 and 13, respectively, as a function of the occupation. From these figures, one can see that for most of the occupation numbers, the MAE changes have opposite sign for the opposite orientation when the electric field is reversed. The origin of these changes of the MAE can be attributed first of all to the modification of the electronic structure of the Pt film, i.e., the electric field controlled hybridization of the d and p orbitals, as discussed in Ref. [19].

IV. CONCLUSIONS

In conclusion, in this work we examined the influence of an electric field effect on the magnetic properties in the Pt layer of $Pd(001)/Co_n/Pt_m$ thin film structures by performing first-principles calculations. For this purpose, a homogeneous external electric field was modeled by a charged plate in front of the surface. From the self-consistent calculations, we determined the spin magnetic moment and XMCD spectra in the presence of an electric field. We found that in the case

of $Pd(001)/Co_2/Pt_2$ and $Pd(001)/Co_5/Pt_2$, the spin-magnetic moments are varying independently from the number of Co layers and not linearly as a function of the electric field strength. An inspection of the angular momentum resolved DOS reveals that the electric field slightly shifts the s and p states around the Fermi level. From the calculated XMCD spectra, it was found that the electric field has its major impact for the L_3 edge spectra. We also investigated the dependency of the electric field effect on the thicknesses of the Pt layer. In the case of $Pd(001)/Co_5/Pt_1$ as well as $Pd(001)/Co_5/Pt_4$, the electric-field-induced change of the XMCD spectra is most significant for the L_3 edge, independent of the thickness of the Pt capping layer. In addition, the layer-dependent MAE and its dependency on an electric field were examined. It was found that the electric field strongly modifies the MAE. It turned out in particular that this change is still considerable for deeper-lying layers.

Our work is mainly motivated by the recent experimental XMCD study in Ref. [13], and we performed detailed theoretical calculations to investigate the electric field effect for the Co/Pt system. Beyond the technological interest in the Co/Pt system, our study provides more insight into the effect of an external electric field on magnetism. We expect that the present work may motivate further experimental investigations via XMCD measurements to explore the effect of an electric field for different systems.

APPENDIX: TORQUE METHOD

Considering the ferromagnetically ordered system with the magnetization oriented along the direction $\hat{n} = (\theta, \phi)$, the torque on the magnetic moment, $T_{\hat{u}}(\theta, \phi) = \mathcal{T}_{\hat{u}}^{\hat{n}} = \vec{\mathcal{T}}^{\hat{n}} \cdot \hat{u}$, is calculated within the multiple scattering formalism by using the expression based on Lloyd's formula and is given by the expression [34,35]

$$\mathcal{T}_{\hat{u}}^{\hat{n}} = \sum_i \left[-\frac{1}{\pi} \text{Re} \, \text{Tr} \int^{E_F} dE \, \underline{\tau}_{ii}^{\hat{n}} (\hat{u} \cdot \underline{\hat{J}})(\underline{t}_i^{\hat{n}})^{-1} \right.$$
$$\left. - (\underline{t}_i^{\hat{n}})^{-1}(\hat{u} \cdot \underline{\hat{J}}) \right]. \tag{A1}$$

Here $\hat{u}$ specifies the direction of the calculated magnetic torque, which is perpendicular to the rotation plane of magnetization, and $\underline{\hat{J}}$ is the angular momentum operator. The matrices $\underline{t}_i^{\hat{n}}(E)$ and $\underline{\tau}_{ii}^{\hat{n}}(E)$ are the single-site t-matrix and the site diagonal scattering path operator, respectively, where the index i labels the atomic sites in the unit cell.

The torque was calculated for $\phi = 0$, assuming weak anisotropy within the plane perpendicular to the c axis. In this case, taking $\theta = \pi/4$, the value for $T_{\hat{u}}(\pi/4, 0)$ gives immediately the energy for uniaxial anisotropy [34] as discussed in this work.

[1] G. A. Prinz, Science **282**, 1660 (1998).

[2] O. O. Brovko, P. Ruiz-Díaz, T. R. Dasa, and V. S. Stepanyuk, J. Phys.: Condens. Matter **26**, 093001 (2014).

[3] H. Zhang, M. Richter, K. Koepernik, I. Opahle, F. Tasnádi, and H. Eschrig, New J. Phys. **11**, 043007 (2009).

[4] I. Dzyaloshinsky, J. Phys. Chem. Solids **4**, 241 (1958).

[5] T. Moriya, Phys. Rev. Lett. **4**, 228 (1960).

[6] H. Katsura, N. Nagaosa, and A. V. Balatsky, Phys. Rev. Lett. **95**, 057205 (2005).

[7] D. Chiba, M. Sawicki, Y. Nishitani, Y. Nakatani, F. Matsukura, and H. Ohno, Nature (London) **455**, 515 (2008).

[8] Y. Yamada, K. Ueno, T. Fukumura, H. T. Yuan, H. Shimotani, Y. Iwasa, L. Gu, S. Tsukimoto, Y. Ikuhara, and M. Kawasaki, Science **332**, 1065 (2011).

[9] T. Lottermoser, T. Lonkai, U. Amann, D. Hohlwein, J. Ihringer, and M. Fiebig, Nature (London) **430**, 541 (2004).

[10] A. J. Hearmon, F. Fabrizi, L. C. Chapon, R. D. Johnson, D. Prabhakaran, S. V. Streltsov, P. J. Brown, and P. G. Radaelli, Phys. Rev. Lett. **108**, 237201 (2012).

[11] D. Lebeugle, A. Mougin, M. Viret, D. Colson, and L. Ranno, Phys. Rev. Lett. **103**, 257601 (2009).

[12] P. Babkevich, A. Poole, R. D. Johnson, B. Roessli, D. Prabhakaran, and A. T. Boothroyd, Phys. Rev. B **85**, 134428 (2012).

[13] K. T. Yamada, M. Suzuki, A.-M. Pradipto, T. Koyama, S. Kim, K.-J. Kim, S. Ono, T. Taniguchi, H. Mizuno, F. Ando, K. Oda, H. Kakizakai, T. Moriyama, K. Nakamura, D. Chiba, and T. Ono, Phys. Rev. Lett. **120**, 157203 (2018).

[14] A. Obinata, Y. Hibino, D. Hayakawa, T. Koyama, K. Miwa, S. Ono, and D. Chiba, Sci. Rep. **5**, 14303 (2015).

[15] P.-J. Hsu, A. Kubetzka, A. Finco, N. Romming, K. von Bergmann, and R. Wiesendanger, Nat. Nanotechnol. **12**, 123 (2017).

[16] M. Schott, A. Bernand-Mantel, L. Ranno, S. Pizzini, J. Vogel, H. Béa, C. Baraduc, S. Auffret, G. Gaudin, and D. Givord, Nano Lett. **17**, 3006 (2017).

[17] H. Yang, O. Boulle, V. Cros, A. Fert, and M. Chshiev, Sci. Rep. **8**, 12356 (2018).

[18] C.-G. Duan, J. P. Velev, R. F. Sabirianov, Z. Zhu, J. Chu, S. S. Jaswal, and E. Y. Tsymbal, Phys. Rev. Lett. **101**, 137201 (2008).

[19] K. Nakamura, R. Shimabukuro, Y. Fujiwara, T. Akiyama, T. Ito, and A. J. Freeman, Phys. Rev. Lett. **102**, 187201 (2009).

[20] D. Chiba, Y. Nakatani, F. Matsukura, and H. Ohno, Appl. Phys. Lett. **96**, 192506 (2010).

[21] D. Chiba, S. Fukami, K. Shimamura, N. Ishiwata, K. Kobayashi, and T. Ono, Nat. Mater. **10**, 853 (2011).

[22] C. Takahashi, M. Ogura, and H. Akai, J. Phys.: Condens. Matter **19**, 365233 (2007).

[23] J. Okabayashi, Y. Miura, and H. Munekata, Sci. Rep. **8**, 8303 (2018).

[24] B. T. Thole, P. Carra, F. Sette, and G. van der Laan, Phys. Rev. Lett. **68**, 1943 (1992).

[25] P. Carra, B. T. Thole, M. Altarelli, and X. Wang, Phys. Rev. Lett. **70**, 694 (1993).

[26] M. Altarelli, Phys. Rev. B **47**, 597 (1993).

[27] A. Ankudinov and J. J. Rehr, Phys. Rev. B **51**, 1282 (1995).

[28] C. Ederer, M. Komelj, M. Fähnle, and G. Schütz, Phys. Rev. B **66**, 094413 (2002).

[29] S. H. Vosko, L. Wilk, and M. Nusair, Can. J. Phys. **58**, 1200 (1980).

[30] H. Ebert, D. Ködderitzsch, and J. Minár, Rep. Prog. Phys. **74**, 096501 (2011).

[31] H. Ebert and R. Zeller, The SPR-TB-KKR package, http://olymp.cup.uni-muenchen.de (2006).

[32] R. Zeller, P. H. Dederichs, B. Újfalussy, L. Szunyogh, and P. Weinberger, Phys. Rev. B **52**, 8807 (1995).

[33] H. Ebert, Rep. Prog. Phys. **59**, 1665 (1996).

[34] J. B. Staunton, L. Szunyogh, A. Buruzs, B. L. Gyorffy, S. Ostanin, and L. Udvardi, Phys. Rev. B **74**, 144411 (2006).

[35] S. Bornemann, J. Minár, J. B. Staunton, J. Honolka, A. Enders, K. Kern, and H. Ebert, Eur. Phys. J. D **45**, 529 (2007).

[36] O. Šipr, J. Minár, S. Mankovsky, and H. Ebert, Phys. Rev. B **78**, 144403 (2008).

[37] G. H. O. Daalderop, P. J. Kelly, and M. F. H. Schuurmans, Phys. Rev. B **50**, 9989 (1994).

[38] D.-s. Wang, R. Wu, and A. J. Freeman, Phys. Rev. B **48**, 15886 (1993).

[39] G. H. O. Daalderop, P. J. Kelly, and M. F. H. Schuurmans, Phys. Rev. B **42**, 7270 (1990).

[40] M. Cinal and D. M. Edwards, Phys. Rev. B **55**, 3636 (1997).

[41] M. Cinal and D. M. Edwards, Phys. Rev. B **57**, 100 (1998).

[42] M. Cinal, J. Phys.: Condens. Matter **13**, 901 (2001).

[43] B. Heinrich and J. Cochran, Adv. Phys. **42**, 523 (1993).

[44] T. R. Dasa, P. Ruiz-Díaz, O. O. Brovko, and V. S. Stepanyuk, Phys. Rev. B **88**, 104409 (2013).

[45] S. Ouazi, S. Vlaic, S. Rusponi, G. Moulas, P. Buluschek, K. Halleux, S. Bornemann, S. Mankovsky, J. Minár, J. B. Staunton, H. Ebert, and H. Brune, Nat. Commun. **3**, 1313 (2012).

[46] P. Beauvillain, A. Bounouh, C. Chappert, R. Mégy, S. Ould-Mahfoud, J. P. Renard, P. Veillet, D. Weller, and J. Corno, J. Appl. Phys. **76**, 6078 (1994).

[47] B. Újfalussy, L. Szunyogh, P. Bruno, and P. Weinberger, Phys. Rev. Lett. **77**, 1805 (1996).

[48] C. Andersson, B. Sanyal, O. Eriksson, L. Nordström, O. Karis, D. Arvanitis, T. Konishi, E. Holub-Krappe, and J. H. Dunn, Phys. Rev. Lett. **99**, 177207 (2007).

[49] O. Jun, K. Tomohiro, S. Motohiro, T. Masahito, S. Masafumi, and C. Daichi, Sci. Rep. **7**, 46132 (2017).